Wear 368-369 (2016) 314–325

Contents lists available at ScienceDirect

Wear

journal homepage: www.elsevier.com/locate/wear

A prototype of on-line extraction and three-dimensional characterisation of wear particle features from video sequence

Hongkun Wu [a,*], Ngai Ming Kwok [a], Sanchi Liu [a], Tonghai Wu [b], Zhongxiao Peng [a]

[a] School of Mechanical and Manufacturing Engineering, the University of New South Wales, Sydney, NSW, 2052, Australia
[b] Key Laboratory of Education Ministry for Modern Design and Rotor Bearing System, Xi'an Jiaotong University, Xi'an, 710049, China

ARTICLE INFO

Article history:
Received 19 June 2016
Received in revised form
22 September 2016
Accepted 26 September 2016
Available online 30 September 2016

Keywords:
Particle shape
Ferrography
Optical microscopy
Wear testing

ABSTRACT

Wear particles in lubricants carry valuable information about machine wear status which is useful in machine condition monitoring. For wear analysis, wear particles are often imaged and their features are extracted. However, the particle morphology acquired from current 2-dimensional (2-D) images does not contain thickness information which can be critical in wear mechanism interpretation. In this paper, we present the development of a video based system to extend the particle information in 3-dimension (3-D). The proposed method contains three main procedures including: particle extraction using a Gaussian mixture model, multiple particle tracking with Kalman filter, and 3-D feature reconstruction by the shape-from-silhouette method. This framework ensures that wear particles are correctly extracted, and their 3-D morphological features are obtained. It also can be regarded as a potential option for on-line particle monitoring. The performance of this method was demonstrated by analysing wear particles generated from a four-ball machine and a spur gear box, and verified by computer simulations. Results indicated that 3-D features of wear particles were obtained with satisfactory accuracy.

1. Introduction

Condition monitoring can provide valuable insights regarding the machine running states, enabling the prediction of operation lifespan and the formulation of proper maintenance schedules for economic operation. Since it is an inherent phenomenon that wear occurs in a machine, wear particles can be used to examine the cause of a fault or the eventual failure of machine [1]. Among the various methods of particle monitoring, image based wear particle analysis is regarded as a promising technique. By investigating morphological features of wear particle, wear mechanisms can be inferred [2].

Generally, information observed from the wear particle image can be grouped into statistical and individual data. The first category includes indicators such as the number of particles, their concentration, and size distribution, from which wear severity and wear rate can be estimated [3]. Moreover, individual wear particle can be further characterised using its 2-D morphological features [2,4,5]. While the morphological data of individual particle providing insight to wear mechanism information, 2-D features alone are insufficient for the classification of particle shapes into fatigue chunk, laminar and sphere [6]. This is because 2-D image only provide the particle information facing the camera without capturing the particle data in thickness.

To explore particle morphology in higher dimension, three instruments including laser scanning confocal microscopy (LSCM), scanning electron microscope (SEM) and atomic force microscope (AFM) have been applied to investigate 3-D particle information [7–9]. The results indicated that 3-D wear particle analysis can provide more morphological information than conventional 2-D methods. However, since the particle is fixed on the slide, these instruments can only capture the particle information on one side, which means the particle thickness is still partially obtained. Furthermore, these lab-based facilities can be expensive and not suitable to be used on site [10].

Video based methods were developed to investigate more detailed particle features in recent years [11,12]. The principle of these video techniques are similar. The wear particles are collected by a flow channel, on which a camera is mounted to capture the video of particle in the flowing lubricant. Features of individual particle such as colour has been extracted to investigate the particle oxidation [13]. In addition, this methodology has also been applied to estimate 3-D particle information, which was a very promising attempt since it extended particle analysis to two views [12]. However, as claimed by the developer, the obtained 3-D model was not a full reflection of the particle because only two artificially selected images are considered. Furthermore, the need

* Corresponding author.
E-mail address: hongkun.wu@student.unsw.edu.au (H. Wu).

http://dx.doi.org/10.1016/j.wear.2016.09.024
0043-1648/

for manual operation also limits its efficiency in multiple particle analysis. As a result, a method for comprehensive 3-D wear particle image acquisition and description is necessary.

Conducting wear analysis in short time interval is a commonly preferred approach, to obtain timely indication on machine health conditions [14–18]. Although the aforementioned developments have accomplished their individual goals, an efficient 3-D wear particle characterisation has not been fulfilled. As a result, we develop a wear particle extraction and reconstruction technique to further improve 3-D particle analysis. This technique contains three parts, particle extraction, particle tracking and 3-D particle reconstruction.

Firstly, as Gaussian mixture modelling has been proved to be an efficient and robust technique for recognising object from real-time surveillance videos, it is used to expose wear particle from the captured video [19]. Next, the particles in the video are tracked to collect their profiles in multiple views. To ensure the tracking reliability, the particle motion is estimated with Kalman filter, which is extensively employed in object tracking area such as traffic management and robot navigation [20,21]. After successfully identified and tracked the particle in multiple views, 3-D representation of the particle is reconstructed. Based on contour information, shape-from-silhouette (SFS) is an effective technique to reconstruct 3-D object without detailed information about every pixel [22,23]. As a result, SFS is applied to construct 3-D particle. Verifications are then conducted to evaluate the effectiveness of the proposed automatic technique for 3-D wear particle description.

The rest of the paper is organized as follows. In Section 2, the extraction of particle is detailed. The Gaussian mixture model is briefly presented and its implementation is described. In Section 3, the need for wear particle tracking is highlighted together with the development outline of the tracking processes employing the Kalman filter. Section 4 presents the silhouette based 3-D wear particle reconstruction with an example. Verification and the experimental results are given in Section 5. Section 7 contains the conclusions drawn.

2. Particle extraction from on-line wear particle video

The first step of wear particle analysis is extracting the particle from the captured video. While there are existing segmentation-based particle extraction methods for static images used in ferrograph based analysis, they are not directly applicable to video streams which are composed of moving objects and variant background. Therefore, a particle segmentation method for extracting particle from the on-line particle video needs to be devised.

Background subtraction was reported to extract wear particle from on-line particle video [11,24]. This method allows the separation of particles from frames with similar backgrounds. However, the need of a manually calibrated background and a fixed differentiate threshold may limit its applicability in variant particle background, which is commonly observed due to the oxidation and contamination of lubrication oil. Therefore, an adaptive particle extraction strategy is preferred.

An adaptive particle extraction method based on Gaussian Mixture Modelling (GMM) is developed to extract wear particle from the on-line video. This method estimates the foreground and background pixel by pixel with a statistical modelling process [19]. Its basic principle is presented as followed.

2.1. Gaussian mixture modelling of pixel intensity

The intensity of a pixel $\{x_p, y_p\}$ in on-line particle video can be considered as a process $\{\mathcal{I}_1, \ldots, \mathcal{I}_t\}$. In addition, the intensity distribution of a recently observed pixel is modelled by a mixture of Gaussian functions. The parameters of the Gaussian functions are highly related to the properties of particle or background. For example, the pixel value of background is often stable, this results in a Gaussian function with small variance. While the result of particle pixel as foreground is versa. Based on the mixture model, one can tell the probability of a pixel belonging to background or foreground, and enable the particle to be extracted. A detailed description of the GMM modelling process is given in Appendix A.

2.2. Wear particle extraction based on gaussian mixture modelling

With the pixel intensity modelled by a combination of 3 Gaussian distributions, the particle segmentation from on-line video can be achieved by dividing all the pixels into two groups: background pixels and the particle pixels. To determine which group a pixel belongs, three main steps will be carried out: (1) estimation of background Gaussian; (2) pixel matching with Gaussian models; and (3) update of Gaussian models.

2.2.1. Background model estimation of particle video

The estimation of background model is to determine which Gaussian distribution is more probably to be produced by the background process. As observed from on-line wear particle video, a background pixel generally has a lower intensity variance, σ^2, than particle pixel. Furthermore, the weight of the background distribution, ω, will accumulate by an updating rule given in Section 2.2.3. Therefore, one can tell which Gaussian is the background distribution according to the ratio of weight and variance, ω/σ^2.

2.2.2. Pixel matching with gaussian models

The extraction of wear particle from on-line video is conducted by matching the pixel and the background model obtained in Section 2.2.1. The pixel X_t is called matched with a Gaussian model $\mathcal{N}_j$ if

$$|\mathcal{I}_t - \mu_{j,t}| \leq 2.5 \times \sigma_{j,t}. \quad (1)$$

The pixel matched to any background Gaussian is deemed to be an background pixel. The unmatched will be regarded as a particle pixel.

2.2.3. Parameters update for mixture gaussian model

The GMM method iterates by updating the parameters with pixel from new frames. Based on the matching result, the parameters of the Gaussian distributions will be updated by adjusting the model weight, mean value and variance.

2.2.4. Experiment of GMM based particle extraction

The developed GMM wear particle extraction method is tested against wear particle videos under different illumination conditions. The oil samples are collected from a four-ball machine wear test and a spur gear box wear test. The lubrication used is Magnetic Synthetic Engine Oil ($SAE15W-40$). The test balls used are bearing steel ball which are manufactured of carbon chromium bearing steel ($GCr15$), with a surface roughness of 0.025 mm and a hardness falling in $HRC58 \sim 63$. The test gears are manufactured of $S45C$ carbon steel with a surface hardness less than $HB194$. The resolution of the captured video is 800×600 pixels, and its frame rate is 15 per second. The pseudo code of the particle extraction process is detailed in Appendix A. According to the computation result obtained from a personal computer ($IntelCorei5-4750\ CPU$, $16\ GB\ RAM$, $Matlab\ 2015b$, $Windows764-bit\ OS$), the computation time for extracting particle from one frame is

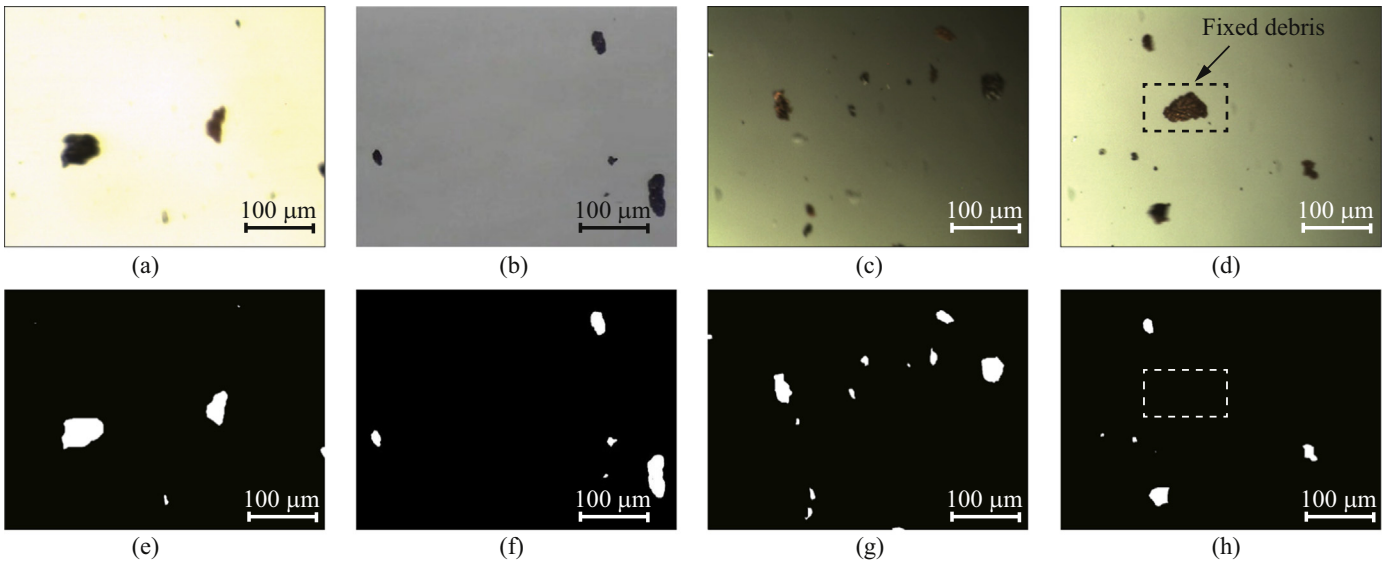

Fig. 1. GMM based background detection, (a) particle video of four-ball machine lubricant oil; (b) particle video of spur gear box lubricant oil; (c) particle video under improper illumination; (d) particle video with fixed wear particle; (e) particle detection of video in (a); (f) particle detection of video in (b); (g) particle detection of video in (c); (h) particle detection of video in (d).

about 0.035 s, which means that it can provide an immediate result before the next frame is input. The particle extraction result is shown in Fig. 1, in which black part indicates background area and white parts indicate particles detected.

As can be observed from the figure, the wear particles have been successfully extracted from video under different illumination scenario. However, one limitation of this method is that particles remain stationary for a long period(≥50 *frames*) would merge into background, as shown in Fig. 1(d), and (h). While it is tolerable since most particle in the video are continuously moving. As can be concluded, the self adaptivity of this method allows it to maintain robust performance under different scenarios. This method is more suitable for on-line wear particle extraction since dose not require any manually initialized backgrounds.

3. Wear particle tracking

Wear particle video carries particle information with a series of multi-view images. Because the image of a wear particle in each frame only display the particle in one view direction, all the images of particle in different views should be incorporated to conduct full particle description. Therefore, a particle tracking method is developed to fulfill multi-view analysis of each wear particle in the video.

According to the number of tracking object, on-line wear particle tracking can be defined as a multi-object-tracking (MOT) issue concerned with tracking multiple moving targets [25,26]. This section will present the construction of a Kalman-filter based particle tracking method in three stages: (1) particle representation; (2) particle motion estimation; (3) data association of multiple particles.

3.1. Wear particle representation

The particle representation is to abstract the particle appearance by defining a parameters space for further tracking. The tracking target can be represented by points, shapes, contour and surface features [26]. Generally, the most desirable property of a parameters space is its uniqueness so that the objects can be easily distinguished. Because most of the particles in on-line video merely occupy small regions, a points representation called centroid is applied to identify the particles position.

However, the particle centroid will shift in different frames due to the particle rotation, making the centroid representation not able to accurately indicate the particle position. Therefore, more features should be incorporated. As the longitude axis of a particle is relative stable when the particle is rotating, it is combined with the particle centroid to represent wear particle for tracking. Thus, the wear particle representation model for tracking is defined as

$$\mathcal{W} = \left[C_x, C_y, \mathcal{L} \right]^{\mathrm{T}}, \tag{2}$$

where C_x and C_y is the particle centroid, and $\mathcal{L}$ is the particle longitude axis. It should be noted that this representation is defined to help identifying an individual particle, instead of a comprehensive morphological description.

3.2. Motion estimation of wear particle

The particle motion estimation is the critical step in particle tracking, which helps to determine the particle location dynamically by constructing a motion model for each moving particle. In the fluid channel, the motion of a wear particle is a combination of several forces, among which viscous drag is the dominate one [17]. As the magnitude of viscous drag is heavily dependent on the area where the force acts, the motion of wear particles can be quite diverse due to the wide range of particle dimension. Furthermore, the motion speed of particles located in the middle of the channel is higher than those around the channel boundary. All these factors contribute to the uncertainties in particle motion in the video an uncertain process. To reliably locate the moving particle, the motion of each particle will be estimated.

In our system, a Kalman filter based estimation method is developed to explore the motion of wear particle in the video. The estimation begins by defining a state space describing the motions of the particle. We define the state space of moving particle at time t as

$$\mathbf{x}^t = \left[C_x^t, d_{C_x^t}, C_y^t, d_{C_y^t}, \mathcal{L}^t, d_{\mathcal{L}^t} \right]^{\mathrm{T}}, \tag{3}$$

where $d_{C_x^t}$, $d_{C_y^t}$ and $d_{\mathcal{L}^t}$ are differential of the state components over time t. Based on this state space, the motion estimation of single

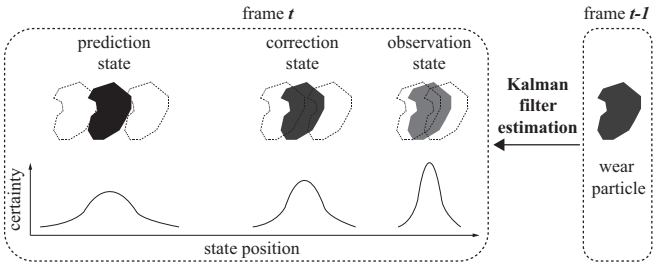

Fig. 2. Kalman filter based motion estimation of single wear debris.

wear particle will be introduced as: prediction, observation and correction in a Kalman filter process [21]. With the motion estimation shown in Fig. 2, the motion process is briefly presented as following.

Prediction step: the position of a particle in frame t can be predicted by its determined position in time $t-1$. Because the flow rate of the lubricant is constant, we use a constant velocity model to predict particle position across frames.

Observation step: the observation is performed based on the segmentation result. Because the video sensor can only obtain the position and shape of particle, three indicators including ${C_x}^t$, ${C_y}^t$ and $\mathcal{L}^t$ are extracted to form the particle observation at time t.

Correction step: with the prediction and observation obtained, the position of wear particle in time t can be corrected. By considering the uncertainty of each item, a more accurate estimation of particle position in time t can be generated.

Detail description of these three stages are given in Appendix B. The iteration of the three steps allows one to tell the position of the moving particle, which will help to extract image of individual wear particle in different frames. Such motion estimation will be conducted in parallel for all the particles for multi-view images extraction.

3.3. Data association of multiple wear particles

In on-line wear particle videos, we are interested in exploring more than one wear particle in each frame. Data association is a process that enables the tracking of multiple wear particle simultaneously. Different from the tracking of individual particle, multiple particles tracking will generate more than one prediction and observation states in each frame. We, therefore, need to associate each observation to its corresponding prediction to estimate the position of each particle.

3.3.1. Distance based association for multiple wear particles

The data association method used in our system is called nearest neighbour standard filter (NNSF) [27]. The principle is briefly illustrated as follows. $\{\mathbf{x}_{c1}^{t-1}, \mathbf{x}_{c2}^{t-1}\}$ are two corrected wear particle in time $t-1$; $\{\mathbf{x}_{p1}^{t|t-1}, \mathbf{x}_{p2}^{t|t-1}\}$ are two predicted results from $\{\mathbf{x}_{c1}^{t-1}, \mathbf{x}_{c2}^{t-1}\}$ at time $t-1$; $\{\mathbf{z}_1^t, \mathbf{z}_2^t\}$ are two observed wear particle in time t. The correspondence relationship between the prediction $\{\mathbf{x}_{p1}^{t|t-1}, \mathbf{x}_{p2}^{t|t-1}\}$ and the observation $\{\mathbf{z}_1^t, \mathbf{z}_2^t\}$ can be determined by the distance measured. In particular, a prediction and an observation share the least distance will be associated.

In the fluid channel, the motion directions of most particles are consistent with the flow direction, which is parallel to the fluid channel. Such motion will result in larger uncertainty of prediction and observation in the direction parallel to the channel. *Mahalanobis distance*, $\mathcal{D}_M$ is, therefore, used to describe the distance to account for the uncertainties of prediction $\mathbf{x}_p^{t|t-1}$ and observation $\mathbf{z}^t$:

$$\mathcal{D}_M(\mathbf{x}_p^{t|t-1}, \mathbf{z}^t) = \sqrt{(\mathbf{x}_p^{t|t-1} - \mathbf{z}^t)^{\mathrm{T}}(\mathbf{H}\mathbf{P}^{t|t-1}\mathbf{H}^{\mathrm{T}} + \mathbf{R}^t)^{-1}(\mathbf{x}_p^{t|t-1} - \mathbf{z}^t)}, \quad (4)$$

where $\mathbf{H}$ is the measurement matrix; $\mathbf{P}^{t|t-1}$ is the uncertainty of prediction; $\mathbf{R}^t$ is related to the uncertainty of observation.

According to Eq. (4), the $\mathcal{D}_M$ will compress the space in the direction of large covariance. Even if the Euclidean distances between the prediction $\mathbf{x}_p^{t|t-1}$ and two observations $\mathbf{z}_1^t$, $\mathbf{z}_2^t$ are similar, $\mathbf{x}_p^{t|t-1}$ will be associated with the observation $\mathbf{z}_1^t$ with a smaller $\mathcal{D}_M$. With the prediction and observation uncertainty taken into account, the predictions and observations of wear particles in each video frame can be associated robustly.

3.3.2. Data association in multiple particle tracking

In on-line wear particle monitoring, the data association of multiple particles will be conducted in each frame as followed. The information of the particle, with associated prediction and observation states, will be extracted and stored for further analysis. The non-associated prediction is regarded as invalid and is discarded. For the non-associated observation, new prediction will be carried out in next frame.

The tracking result of a particle video captured from the wear test of four-ball machine is shown in Fig. 3. During the tracking process, a tracked particle will be marked with an identification number, as shown in Fig. 3 (a). According to our test, the computation time for tracking particles in each frame is less than 0.040 s. The images series of the tracked wear particle in the video will be saved. These saved images are regarded as the multi-view profiles of each particle, as shown in Fig. 3 (b). The images correlated to each individual wear particles can therefore be identified, labeled and separately stored with our proposed on-line particle tracking processes. Using the obtained image series of individual particle in different views, the three-dimensional modeling of the particle can be conducted.

4. 3-D wear particle reconstruction

The tracking of wear particle provides 2-D particle features from different views. This allows us to characterize the wear particles in 3-D. The 3-D reconstruction principle used in our method is Shape-from-Silhouette (SFS) [22,23]. The shape of a wear particle will be recovered by intersecting the projection from the particle silhouettes in different views. Generally, two steps are involved in SFS: (1) camera parameters determination; and (2) volume intersection.

4.1. Estimation of camera parameters

To reconstruct a 3-D object, the camera information including intrinsic and extrinsic parameters need to be understood and determined [28]. These parameters and their determination procedures are explained below.

The intrinsic properties of a camera is comprised of a set of physical parameters, including the focal length of the lens, the size of the pixels, and the position of the principle point on the image sensor [29]. The intrinsic parameters is represented by a 3×3 matrix $\mathcal{K}$ which is detailed in Appendix C. As the intrinsic parameters remain constant for a given camera, $\mathcal{K}$ is suitable for projecting the wear particle rotating in different views. The intrinsic matrix allows a sense point ${}^{C}\mathcal{P}$ of the particle in the camera coordinates to be projected as a pixel, $\mathcal{P}$, in the image coordinates.

The properties of camera in the world coordinates, such as pose and orientation are represented as extrinsic parameters. In particular, the sense point ${}^{W}\mathcal{P}$ of wear particle in the world coordinates can be projected to a point ${}^{C}\mathcal{P}$ in camera coordinates. A more

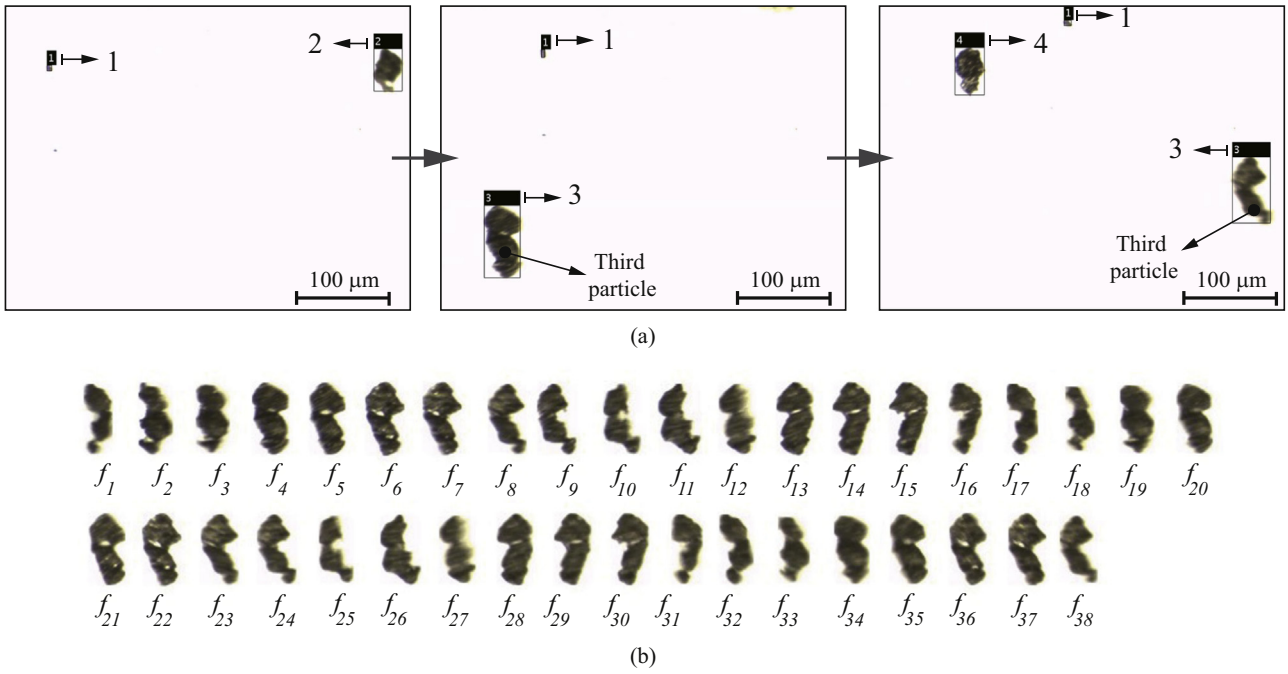

Fig. 3. Multiple wear particle tracking, (a) corresponding tracked wear particle with mark number; (b) tracking series of individual wear particle.

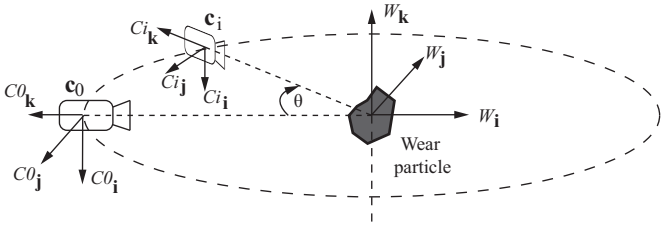

Fig. 4. Geometric relationship between word coordinate and camera coordinate.

detailed illustration of the extrinsic parameters and the projection process is given in Appendix C.

To determine the extrinsic parameters, the geometric relationship between the particle and the camera need to be understood. For this particle sensor, wear particle is rotating in the fluid channel while the camera is fixed. Therefore, the motion relationship between the camera and wear particle can be viewed as a stationary particle being imaged by a camera cycling around it. As a result, the relationship of pose and orientation between the particle and the camera is illustrated as Fig. 4.

Since the distance between the camera and fluid channel is fixed and is much larger than the channel thickness, the distance between the particle and camera can also be approximated as constant. Therefore, the orientation of each profile is required to determine the extrinsic parameters. As shown in Fig. 4, by assuming the orientation of camera $\mathbf{c}_0$ as the initial orientation, the orientation of camera $\mathbf{c}_i$ can be obtained according to the rotation angle θ. The calculation of extrinsic parameters with rotation angle θ is detailed in Appendix C. As a result, to obtain the extrinsic parameters, the rotation steps between of all profiles should be known.

4.2. Determination of rotation step

In the fluid channel, wear particle rotates due to the viscous drag of the lubricant. According to the observation of 192 wear particles from six videos, 169 (88%) particles are rotating in the channel, while the rest are not. This result agreed with those reported in [12]. Since the lubrication flowing speed is constant, the particle rotation is consequently stable. In particular, among the rotating particles, 66% are rotating with approximately constant speed, while the rest particles rotate with random speed. Fig. 3 (b) presents the tracked profile sequences of a rotating particle. To determine the rotation of each particle profile, the frame series corresponding to one rotation cycle will be extracted first; the rotation angles of those extracted profiles then will be estimated.

As the wear particles are rotating in the channel, the features of the wear particles in the frame would vary periodically. Frames with similar morphological features to the first captured frame are identified as the initial frame of each subsequent rotations. Based on the tracking results shown in Fig. 3(b), the process to identify the image series of one rotation cycle is presented as follows:

a. The first frame of the tracked result shown in Fig. 3(b) is regarded as the initial frame of the first rotation cycle.
b. The subsequent frames are compared with the initial frame by differentiating the *invariant moments* (IM) of the image, which is a commonly applied imaging matching approach [30]. The frame with the closest IM value to that of the first frame is regarded as the matched one and is set as the initial frame for the next rotation cycle. The differential result of the tracking series to the initial frame is shown in Fig. 5 (a). As observed, the 17th frame is matched.
c. Finally, any frames before the matched frame will be labelled as the frames in the first rotation cycle, as shown in Fig. 5 (b).

After the particle profiles within one rotation cycle are obtained, we can estimate the rotation step size. As the wear particle is rotating, it will display different profiles in the video. The morphological discrepancy between two neighbouring frames therefore is used to approximate the rotation angle. To characterise the profile information carried by a frame f_i, six morphological features including area, minor axis, aspect ratio, eccentricity, perimeter, equivalent diameter are incorporated to formulate a morphological vector, $\mathbf{mf}_i$. The rotation angle $\bar{\theta}_i$

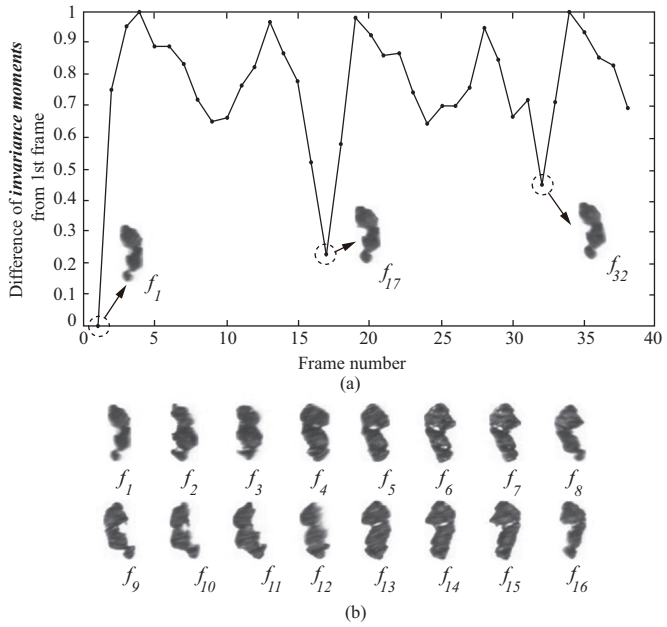

Fig. 5. Frame match to the initial frame.

Table 1
Rotation angle of image series in Fig. 5(b).

Frame	1	2	3	4	5	6	7	8
$\bar{\theta}/°$	0	35.4	54.8	81.9	101.3	121.0	129.1	147.6
Frame	9	10	11	12	13	14	15	16
$\bar{\theta}/°$	168.2	189.6	212.9	249.2	295.2	308.5	313.6	348.2

between frame i-1 and frame i is then calculated as

$$\bar{\theta}_i \approx \frac{\| \mathbf{mf}_i - \mathbf{mf}_{i-1} \|_2}{\sum_{j=1}^{N} \| \mathbf{mf}_{j+1} - \mathbf{mf}_j \|_2} \times 360°,\ i = 2, 3, \ldots, N, \tag{5}$$

where N is the number of frames in the rotation cycle; and $\bar{\theta}_1$ is 0. The rotation step sizes $\bar{\theta}$ of the frame series shown in Fig. 5 (b) are listed in Table 1.

With the approximated rotation step size $\bar{\theta}$, the extrinsic matrix of a particle in different views can be determined. As a result, the volumetric reconstruction of the 3-D wear particle can then be performed.

4.3. Particle reconstruction by volume intersection

Volume intersection is the combination of particle cross-sections from different views. This method is regarded as a reversal process of the image capturing from an object [23]. By projecting the inner area of particle profiles to 3-D world, one can determine the shape of 3-D particle. Detail description of the volume intersection can be found in Appendix C. The process of 3-D wear particle reconstruction is presented in this section.

4.3.1. Configuration of camera and initial volume

The voxel carving of wear particle is based on the frame series shown in Fig. 5 (b). The carving operation will be conducted with 16 particle silhouettes. The configuration of camera and initial volume is presented in Fig. 6. In order to conduct the projection from the initial volume to the silhouette, V is digitalized to a $Q_r \times Q_r \times Q_r$ discrete matrix $\mathbf{V}_D$, where Q_r denotes the number of points in each edge. A larger Q_r allows for more details in the carved particles, but the calculations involved would be more

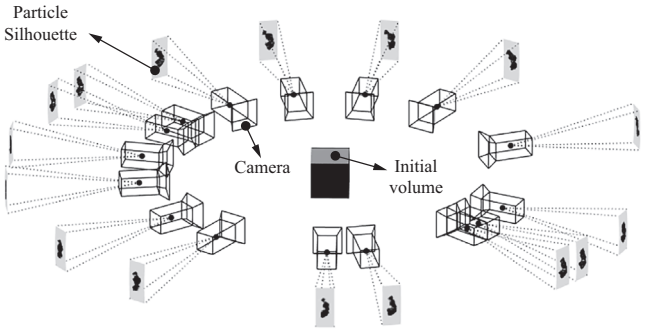

Fig. 6. Configuration of camera and initial volume.

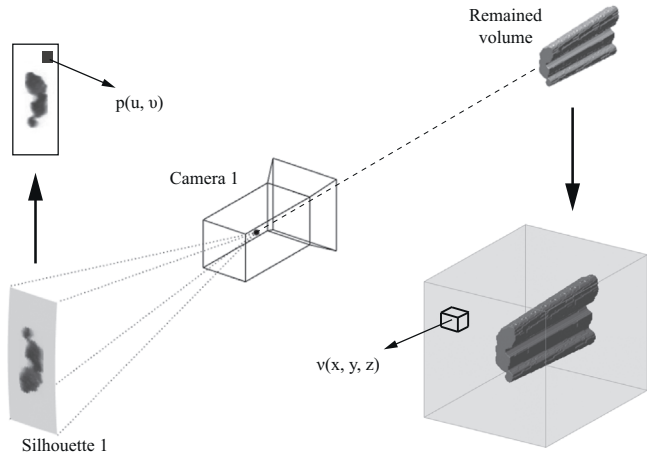

Fig. 7. Space carving with one silhouette.

computationally expensive. Therefore, Q_r is set as 100 in our algorithm to achieve a balance between particle details and computational efficiency. The initial volume is then represented by some basic regular tessellation of cube, known as voxels: $\nu(x, y, z)$.

4.3.2. Space carving with one silhouette

The carving process starts from the carving of $\mathbf{V}_D$ by the first silhouette and camera, as shown in Fig. 7. Based on the camera parameters, the voxels $\nu(x, y, z)$ in $\mathbf{V}_D$ are projected back into the image plane with the geometric relationship detailed in Appendix C, which will result in a pixel $p(\mu, \upsilon)$. If the projected pixel p lay outside the silhouette, the corresponding voxel ν is regarded as an irrelevant part in the volume and will be carved. In contrast, the relevant voxels will be maintained. By repeating the projection with the rest of the voxels, the remaining volume is the carved result under this silhouette, as shown in Fig. 7.

4.3.3. Space carving with the all the silhouettes

Similar carvings are performed based on the rest of silhouettes. The final carved result is shown in Fig. 8(a). Details of the remained volume in different views are presented in Fig. 8(b). The remaining volume is the approximation of the wear particle. The reconstruction results of several different particles collected from four-ball machine and spur gear box are also given in Fig. 8 (c)–(d). The 3-D features of the reconstructed particles are extracted and listed in Table 2. Parameters L, W, H and V represent the length, width, thickness and volume of a particle separately. AR denotes the aspect ratio. *Height Aspect Ratio*(HAR) is the ratio of the maximum dimension to thickness. Compared with traditional 2-D particle indicators AR, HAR allows us to identify whether the

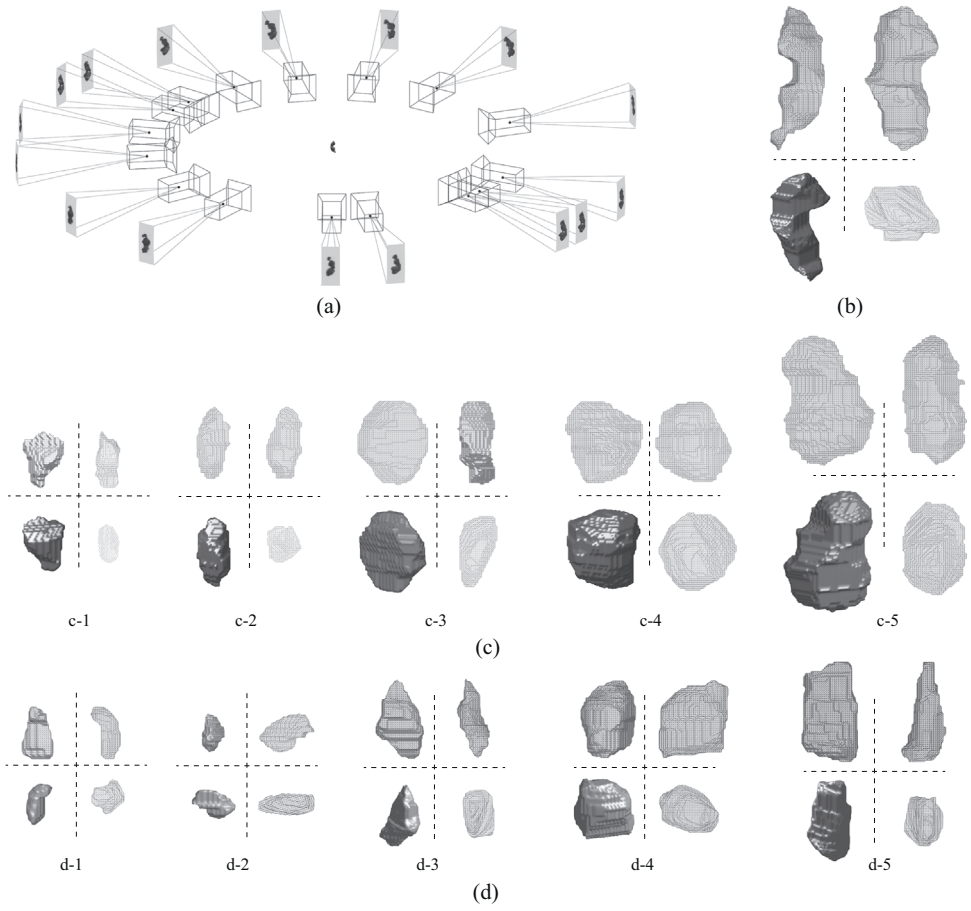

Fig. 8. Space carving with 16 silhouettes, (a) camera configuration and final carving result; (b) amplification of the carving result in different views; (c) reconstruction of particles from four-ball machine test rig; (d) reconstruction of particles from gear test rig.

Table 2
Detail dimension of 3-D reconstructed particle in Fig. 8(b), (c) and (d).

Reconstructed particle in Fig. 8	$L(\mu m)$	$W(\mu m)$	$H(\mu m)$	$V\left(10^3 \mu m^3\right)$	*AR*	*HAR*	Computation cost (*s*)
b	83.65	42.93	31.92	34.26	1.94	2.62	6.182
c-1	31.92	25.70	13.90	4.66	1.24	2.29	4.345
c-2	40.72	19.81	18.71	7.19	2.05	2.17	4.485
c-3	47.32	39.62	20.91	17.74	1.19	2.26	5.732
c-4	46.23	44.03	43.95	41.20	1.04	1.06	6.104
c-5	73.74	52.83	36.32	64.09	1.39	2.03	7.468
d-1	28.62	17.61	15.41	3.03	1.62	1.86	4.583
d-2	29.72	22.01	11.50	3.23	1.35	2.58	7.967
d-3	46.22	28.62	18.71	8.10	1.61	2.47	9.407
d-4	42.93	39.62	27.80	26.30	1.08	1.54	9.389
d-5	57.23	33.02	26.42	21.44	1.73	2.16	8.794

particle is in chunk or laminar shape with the information of thickness. As is known, the fatigue particles which are often generated by crack propagation, are in a chunk shape, while the laminar particle could be produced by the pressing between contacting surfaces [31]. Due to their wear mechanisms, the distinctive feature between them is their thickness. Unfortunately, the traditional 2-D descriptors such as roundness and aspect ratio do not contain the thickness information and thus cannot be used to identify the particles.

As can be observed from Table 2, the proposed method can be applied to investigate particles in more than one view angle, which allows us to differentiate particles with distinct features in thickness. For instance, the two particles shown in Fig. 8(c) can be identified: c-1 is more similar to a laminar one while c-4 approximates a spherical particle. Merely considering 2-D indicator *AR*, the difference is 16%, which is not very significant. In comparison, the difference between their 3-D features, described using the *HAR*, is about 54%, which will help us to recognise their actual difference. A similar result can also be obtained from particles c-3 versus c-4 and c-5 versus d-5. As a result, together with *AR*, the value of *HAR* allows to estimate the closeness of a particle to laminar shape. For instance, a smaller *HAR* may result from a particle as a chunk instead of a thin platelet.

In addition, according to the computation time needed in the reconstruction process listed in Table 2, the processing of a particle cost approximately 10 s. The speed is acceptable, since the video will generally be processed during the sampling interval, which is much longer than the length of the video.

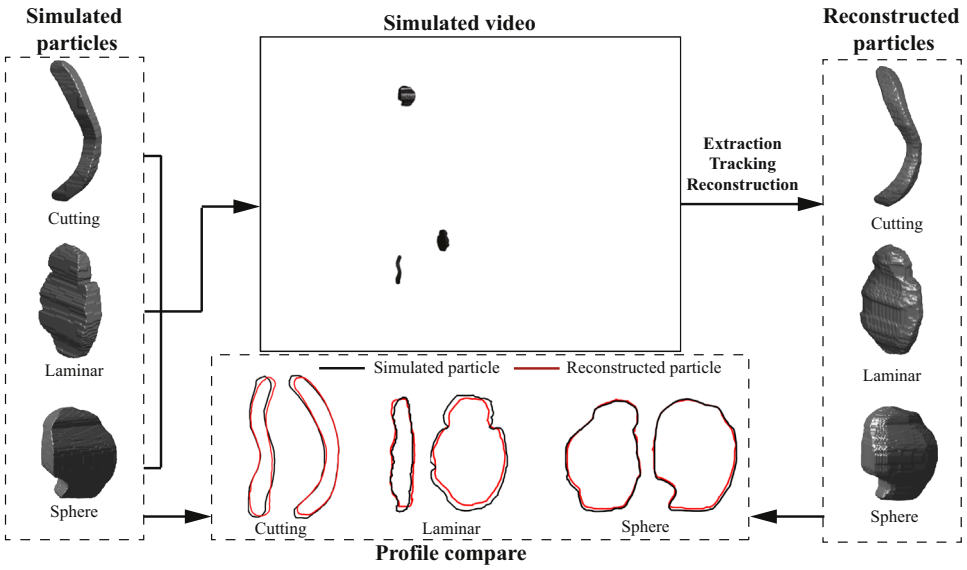

Fig. 9. Verification of wear particle reconstruction.

5. Verification of the method

In this section, we describe a set of experiments performed to verify the performance of the proposed method. First, typical virtual particles are generated as benchmark. In addition, a particle video is simulated by controlling the motion parameters of particle in fluid channel. Finally, the proposed method is applied to obtain 3-D reconstruction of virtual particles. The method is evaluated by comparing the reconstruction result and their corresponding virtual particle. The procedures of the verification are illustrated in Fig. 9.

5.1. Generation of virtual wear particles

An suitable process to evaluate the reconstruction is to compare a reconstructed particle with their respective references, when the 3-D morphologies of the references are known. However, as opposed to measuring the morphology of natural objects, measuring the wear particles in fluid channel could be very challenging. This prevents the relevant information on the reference particles to be obtained. Virtual particles are used to overcome this challenge. For our experiment, three virtual particles are generated by referring 2-D features of typical particles, as shown in Fig. 9. These simulated wear particles are then used as the reference in the verification process.

5.2. Video simulation with multiple moving particles

With the 3-D wear particle simulated, the next step is to generate a video simulating the particle motion in a fluid channel. In particular, the motions are simulated by controlling the motion parameters of particles in six degrees of freedom, including T_x, T_y, T_z, R_x, R_y and R_z, where x is the direction of flow, z is the direction towards the camera, y is the direction perpendicular to both x and z, T denotes translation of the particle and R denote rotation of the particle. Because the distance between the particle and the camera is much larger than the channel thickness, T_z is approximately zero through out the video. Therefore, the translation motion is applied only in the directions of x and y. Since most of the wear particles are observed rotating along the y direction, the mean value of the particle rotation along x and z direction are both set as zero. Three different rotation step in y direction are applied to each particle separately. In addition, noise is also added to each motion parameter to simulate the unknown disturbance. The motion parameters are detailed in Table 3. Finally, a simulated video of wear particles flowing in a fluid channel is synthesized according to the given motion parameters. A frame of the simulated video with three particles is shown in Fig. 9.

Table 3
Motion steps of simulated particle.

Direction	Cutting particle		Laminar particle		Sphere particle	
	Mean	Variance	Mean	Variance	Mean	Variance
$T_x(pixel)$	10	5	16	8	6	3
$T_y(pixel)$	2	2	1	2	1	2
$T_z(pixel)$	0	0	0	0	0	0
$R_x(°)$	0	5	0	5	0	5
$R_y(°)$	20	5	10	5	15	5
$R_z(°)$	0	5	0	5	0	5

5.3. 3-D reconstruction based on the simulated video

The simulated video is regarded as the input to the reconstruction of 3-D wear particles. The particles in the simulated video are detected and tracked to obtain the frame series of each particle in different views. Then the 3-D reconstruction of each particle is conducted based on the frame series. The reconstruction results are shown in Fig. 9. As shown in the figure, typical particle features have been recovered. The difference between the final reconstruction results $\mathcal{F}$ and the original simulated particles O are recorded in Table 4.

As shown in the reconstruction results of the simulated particle, most of the morphological information, including length, width, thickness and aspect ratio are recovered with good accuracy. As a result, the extraction of 3-D indicator, *HAR* is acceptable. However, it can be observed that the feature V indicates relative larger difference compared with the rest features, especially for cutting particle and laminar particle (16%). The main reason of these distinct discrepancies can be understood with the fact that the error in computing V is an accumulation of measuring the

Table 4
A comparison between the simulated particles $\mathcal{O}$ and the reconstructions $\mathcal{F}$.

Features	Cutting particle			Laminar particle			Sphere particle		
	$\mathcal{O}$	$\mathcal{F}$	Error	$\mathcal{O}$	$\mathcal{F}$	Error	$\mathcal{O}$	$\mathcal{F}$	Error
$L(\mu m)$	136.58	135.38	0.88%	102.36	94.66	7.52%	95.76	92.45	3.46%
$W(\mu m)$	48.43	44.03	9.09%	68.24	61.64	9.67%	70.44	68.24	3.12%
$H(\mu m)$	26.42	24.20	8.40%	19.81	20.52	3.58%	63.83	62.74	1.71%
$V(10^3\mu m^3)$	5.14	4.29	16.54%	10.26	8.61	16.08%	33.04	31.16	5.69%
AR	2.82	3.07	8.87%	1.50	1.53	2.00%	1.36	1.35	0.74%
HAR	5.21	5.59	7.29%	5.17	4.61	10.83%	1.50	1.47	2.00%

other three features including *L*, *W* and *H*. As a result, the accuracy of wear rate estimation will be affected. Nonetheless, the identification of laminar particle, chunk particle and sphere particle can be accomplished.

6. Discussion

A strategy for 3-D wear particle characterisation is presented. By incorporating particle profiles in multiple views, we can investigate the thickness and volume information, which are not available by current particle examination approaches based on 3-D images. In particular, this system is composed of three automatic methods including particle extracting, particle tracking and particle reconstruction. According to the robust and efficient real-time performance of those methods in their own area, the developed system is regarded as a potential option for on-line 3-D wear particle characterisation. Compared with the conventional 3-D particle imaging techniques, such as LSCM and SEM, the advantage of this method is that it can capture particle images in different views so the contour information such as particle thickness, can be obtained. However, the on-line image often does not contain sufficient surface information for surface characterisation.

The application of on-line visual ferrograph has validated the feasibility of on-line particle investigation with imaging strategies [17]. According to the analysis results obtained in laboratory using a four-ball machine and a spur gearbox, this method is also able to give particle morphology information in a short time. Due to the limited image resolution, this method allows to examine the morphology of the particles larger than 30 μm. For the small particle less than 30 μm, only particle number can be counted.

In addition, its performance will be affected by image with low quality (normally caused by oil contamination and particle motion), which can be commonly found in some industrial scenario such as the gear box of wind-turbine and marine engine. Therefore, future work will be carried out in on-line wear particle image restoration and enhancement. Although these issues have been rarely addressed in particle image analysis, numerous image processing techniques are available to restore the lost information caused by motion blurring, defocus blurring and contamination [32]. As a result, image restoration and improvement, which have succeeded in related areas, will be conducted to improve the particle image quality.

7. Conclusions

We have presented a video based system for fast 3-D reconstruction of wear particle from 2-D profiles. The objective of this method is to improve the performance of wear particle analysis in on-line condition monitoring by offering more comprehensive wear particle information. The input to our system is wear particle images from multiple views. The main system processes are: 1) dynamical particle extraction with Gaussian mixture modeling; 2) multiple particle tracking for information extraction from individual particle; 3) volumetric reconstruction of wear particle from multiple views. Firstly, the GMM particle extraction method overcame the challenges from illumination variations caused by the deterioration and contamination of lubricant oil. With the adaptability, this method well suited for different cases. Furthermore, image information of individual particle can be automatically extracted by the particle tracking method developed. Finally, wear particle information is extended to the third dimension by reconstructing the required 3-D features. Compared with other particle imaging approaches, this method can provide the thickness information as well as particle volume which can be used to estimate the material loss and wear rate. The automatic process allow fast 3-D particle characterisation, and even make it a potential option for on-line monitoring. However, since our model was only experimented on simulated data for on-line monitoring tests, further verification on industrial machinery is necessary to confirm its capability.

Acknowledgements

The financial support for the present research was provided by the China Scholarship Council (Grant no. 201506280014).

Appendix A. Detail process of GMM based particle segmentation

Gaussian mixture modelling of pixel intensity

The intensity of a pixel $\{x_p, y_p\}$ in on-line particle video can be considered as a process $\{\mathcal{I}_1, \ldots, \mathcal{I}_t\}$. At time t, the probability of observing $\mathcal{I}_t$ at $\{x_p, x_p\}$ can be modelled by a mixture of Gaussian distributions as

$$P(X_t) = \sum_{j=1}^{\mathcal{J}} w_{j,t} \times \mathcal{N}_j\left(\mathcal{I}_t, \mu_{j,t}\Sigma_{j,t}\right). \tag{A.1}$$

Where $w_{j,t}$ is the weight of the j^{th} Gaussian $\mathcal{N}_j$ in the mixture at time t; $\mu_{j,t}$ and $\Sigma_{j,t}$ are the mean and covariance of $\mathcal{N}_j$ in the mixture at time t; $\mathcal{J}$ is the number of Gaussian considered, which is set as 3 in our case.

To guarantee computational efficiency for on-line analysis, the color components, $\mathcal{I}_{c,t}$, $c \in \{R, G, B\}$, of each pixel are considered independent but share the same variance. Therefore, the covariance matrix is defined as

$$\Sigma_{j,t} = \sigma_{j,t}^2 \mathbf{I}, \tag{A.2}$$

where $\mathbf{I}$ is a 3×3 unit matrix, $\sigma_{j,t}^2$ is the unified variance. As a result, the intensity distribution of a recently observed pixel is modelled by a mixture of Gaussian functions.

Pseudo code of GMM based wear particle segmentation

Algorithm 1. Pseudo code of GMM based wear particle segmentation.

Input: Pixel intensity at time t, $\mathcal{I}_t$
Output: Pixel label
1: // *Initialization*
2: Set model weight: $\omega_{j,0} = 0$, (j = 1, 2, 3);
3: Set model means: $\mu_{j,0} = \frac{256}{4} \times j$, ($j$ = 1, 2, 3);
4: Set model variance: $\sigma_{j,0}^2 = 30^2$, (j = 1, 2, 3);
5: **for** t=1; t++ **do**
6: // *Background Gaussian estimation*
7: Sort the Gaussian distributions $\mathcal{N}$ by the ratio $\frac{\omega}{\sigma^2}$ in descending order;
8: The largest B Gaussians are marked as background distributions $\mathcal{N}_b$ by: $B = \arg\min_b\left(\frac{\sum_{j=1}^{b}\omega_{j,t}}{\sum_{j=1}^{3}\omega_{j,t}} \geq 0.7\right)$; the rest Gaussians are marked as $\mathcal{N}_f$;
9: **for** j=1; $j \leq 3$; j++ **do**
10: // *Model matching*
11: **if** $|\mathcal{I}_t - \mu_{j,t-1}| \leq 2.5\sigma_{j,t-1}^2$ **then**
12: $M_{j,t} = 1$, $N_{mg} = N_{mg} + 1$;
13: **if** $\mathcal{N}_j \notin \{\mathcal{N}_b\}$ **then**
14: Pixel label=1;
15: **end if**
16: **else** $M_{j,t} = 0$
17: **end if**
18: // *Model updating*
19: $\omega_{j,t} = (1-\alpha)\omega_{j,t-1} + \alpha M_{j,t}$;
20: $\mu_{j,t} = \mu_{j,t-1} + (\mathcal{I}_t - \mu_{j,t-1})\rho M_{j,t}$;
21: $\sigma_{j,t}^2 = \sigma_{j,t-1}^2 + [(\mathcal{I}_t - \mu_{j,t})^{\mathrm{T}}(\mathcal{I}_t - \mu_{j,t})]M_{j,t}$
22: **end for**
23: **if** N_{mg}=0 **then**
24: update the Gaussian with least $\frac{\omega}{\sigma^2}$ by: $\mu = \mathcal{I}_t$, $\sigma^2 = 30^2$;
25: **else**
26: N_{mg}=0
27: **end if**
28: **end for**

Appendix B. Detail process of wear particle motion estimation

Prediction

The estimation of particle motion is started by predicting the potential position of a particle in time t with its determined position in time $t-1$, which is known as prediction. The prediction process is conducted as

$$\mathbf{x}^{t|t-1} = \mathbf{A}\mathbf{x}^{t-1|t-1} + \mathbf{W}^t. \tag{B.1}$$

$$\mathbf{P}^{t|t-1} = \mathbf{A}\mathbf{P}^{t-1|t-1}\mathbf{A}^T + \mathbf{Q}^t, \tag{B.2}$$

where $\mathbf{A}$ is the state transition matrix which is determined by the moving features of the particle. As the flow velocity of the lubricant is constant, the motion velocity of wear particle is also approximated as constant. Therefore, $\mathbf{A}$ is defined as a constant velocity model which is given as

$$\mathbf{A} = \begin{bmatrix} 1 & 1 & 0 & 0 & 0 & 0 \\ 0 & 1 & 0 & 0 & 0 & 0 \\ 0 & 0 & 1 & 1 & 0 & 0 \\ 0 & 0 & 0 & 1 & 0 & 0 \\ 0 & 0 & 0 & 0 & 1 & 1 \\ 0 & 0 & 0 & 0 & 0 & 1 \end{bmatrix}. \tag{B.3}$$

$\mathbf{W}^t$ is the process noise of each parameters in state, it is assumed to be a zero mean multivariate Gaussian distribution with covariance $\mathbf{Q}^t$. $\mathbf{P}^{t|t-1}$ is the variance associate with the prediction.

Measurement

With the particle segmentation result, three particle indicators including $C_x{}^t$, $C_y{}^t$ and $\mathcal{L}^t$ are extracted to form observation $\mathbf{Z}^t$ of the particle at time t. Therefore, the observation step is defined as:

$$\mathbf{z}^t = \mathbf{H}\mathbf{x}^{re,t} + \mathbf{v}^t, \tag{B.4}$$

where $\mathbf{x}^{re,t}$ is the true state of the particle at time t; $\mathbf{v}^t$ is measurement noise which is assumed to be zero mean Gaussian white noise with covariance $\mathbf{R}^t$; $\mathbf{H}$ is the measurement matrix as:

$$\mathbf{H} = \begin{bmatrix} 1 & 0 & 0 & 0 & 0 & 0 \\ 0 & 0 & 1 & 0 & 0 & 0 \\ 0 & 0 & 0 & 0 & 1 & 0 \end{bmatrix}. \tag{B.5}$$

Correction

The observation of particle state will then be incorporated to correct the prediction result, by

$$\mathbf{K}^t = \mathbf{P}^{t|t-1}\mathbf{H}^{\mathrm{T}}\left[\mathbf{R}^t + \mathbf{H}^t\mathbf{P}^{t|t-1}(\mathbf{H}^t)^{\mathrm{T}}\right]^{-1}, \tag{B.6}$$

$$\mathbf{x}^{t|t} = \mathbf{x}^{t|t-1} + \mathbf{K}^t\left(\mathbf{z}^t - \mathbf{H}\mathbf{x}^{t|t-1}\right), \tag{B.7}$$

$$\mathbf{P}^{t|t} = \left(\mathbf{I} - \mathbf{K}^t\mathbf{H}\right)\mathbf{P}^{t|t-1}, \tag{B.8}$$

where $\mathbf{K}^t$ is Kalman gain, $\mathbf{x}^{t|t}$ is the corrected state, $\mathbf{P}^{t|t}$ is the corrected variance.

Appendix C. Detail information of theory used in 3-D wear particle reconstruction

Intrinsic parameters

In application, the intrinsic parameters of a camera is represented by a 3×3 matrix $\mathcal{K}$:

$$\mathcal{K} = \begin{bmatrix} \alpha & -\alpha\cot\vartheta & \mu_0 \\ 0 & \beta/\sin\vartheta & \upsilon_0 \\ 0 & 0 & 1 \end{bmatrix}, \tag{C.1}$$

where α, β and ϑ are parameters representing optical properties of a pixel; μ_0 and υ_0 are the principle point in the images [29]. After a calibration process, the intrinsic parameters for the imaging device used in our study is determined as: $\alpha = 1744$, $\beta = 1862$, $\vartheta = \pi/2$.

The intrinsic matrix allows a sense point ${}^{C}\mathcal{P} = [{}^{c}x, {}^{c}y, {}^{c}z, 1]^{\mathrm{T}}$ in the camera coordinates to be projected as a pixel, $\mathcal{P} = [\mu, \upsilon, 1]^{\mathrm{T}}$, in the image coordinates, by:

$$\mathcal{P} = \frac{1}{{}^{c}Z}\left[\mathcal{K}\ \mathbf{0}\right]{}^{C}\mathcal{P}. \tag{C.2}$$

Extrinsic parameters of camera $\mathbf{c}_i$

With the extrinsic parameters, the sense point ${}^{W}\mathcal{P}$ in the world coordinates can be projected to a point ${}^{C}\mathcal{P}$ in camera coordinates by the following transformation:

$${}^{C}\mathcal{P} = \mathcal{M}_{E}^{W}\mathcal{P} = \begin{bmatrix} \mathcal{R}_{3\times3} & \mathcal{T}_{3\times1} \\ \mathbf{0}^{\mathrm{T}} & 1 \end{bmatrix}{}^{W}\mathcal{P}, \tag{C.3}$$

where, $\mathcal{M}_E$ is the extrinsic parameter matrix; $\mathcal{R}_{3\times3}$ is a rotational transformation matrix; and $\mathcal{T}_{3\times1}$ is a translational vector.

As shown in Fig. 4, two groups of coordinate base are included, the word coordinates ${}^{W}\mathcal{B} = \left[{}^{W}\mathbf{i}, {}^{W}\mathbf{j}, {}^{W}\mathbf{k}\right]^{\mathrm{T}}$ and the camera coordinates ${}^{C}\mathcal{B} = [{}^{C}\mathbf{i}, {}^{C}\mathbf{j}, {}^{C}\mathbf{k}]^{\mathrm{T}}$. The position and orientation relationship between the two coordinate systems will be explained as following. The camera principle point in world coordinates forms the translational vector $\mathcal{T}$ in Eq. (C.3). The inner product of the two coordinates bases, $[{}^{W}\mathcal{B}\cdot{}^{C}\mathcal{B}^{\mathrm{T}}]$ forms the rotational matrix $\mathcal{R}_{3\times3}$ in Eq. (C.3). For example, The extrinsic parameters of the first camera $\mathbf{c}_0$, as shown in Fig. 4, can be written as:

$$\mathcal{M}_{E}^{0} = \begin{bmatrix} {}^{C0}\mathcal{R}_{W} & \mathcal{T}_{0} \\ \mathbf{0}^{T} & 1 \end{bmatrix}, \tag{C.4}$$

where

$${}^{C0}\mathcal{R}_{W} = [{}^{W}\mathcal{B}\cdot{}^{C0}\mathcal{B}^{\mathrm{T}}],\ \mathcal{T}_{0} = [\,-d\ \ 0\ \ 0]^{\mathrm{T}}. \tag{C.5}$$

$\mathcal{M}_E^0$ represents the extrinsic parameters of the camera $\mathbf{c}_0$, d is the distance between the original point of the two coordinates, which is set as 1 in this system.

As shown in Fig. 4, the extrinsic parameters matrix, $\mathcal{M}_E^i$ of the i^{th} camera rotating by θ about the ${}^{W}\mathbf{k}$ axis can be achieved by multiplying $\mathcal{R}_k(\theta)$

$$\mathcal{R}_{k}(\theta) = \begin{bmatrix} \cos(\theta) & \sin(\theta) & 0 \\ -\sin(\theta) & \cos(\theta) & 0 \\ 0 & 0 & 1 \end{bmatrix}. \tag{C.6}$$

In particular,

$${}^{Ci}\mathcal{R}_{W} = {}^{C0}\mathcal{R}_{W}\cdot\mathcal{R}_{k}(\theta), \tag{C.7}$$

$$\mathcal{T}_{i} = \mathcal{R}_{k}(\theta)\cdot\mathcal{T}_{0}. \tag{C.8}$$

As a result, with a known rotation angle θ, the extrinsic matrix of the i^{th} camera, $\mathcal{M}_E^i$ can be determined.

Principle of space carving

The operation of space carving, is accomplished as a projection process. The space where the object is known to be contained is given as initial volume V. For a particular camera $\mathbf{c}_i$, any world point ${}^{W}\mathcal{P}$ in V can be projected as a pixel $\mathcal{P}$ the image plane of $\mathbf{c}_i$, by

$$\mathcal{P} = \frac{1}{{}^{C}Z}\left[\mathcal{K}_{i}\ \mathbf{0}\right]\mathcal{M}_{Ei}{}^{W}\mathcal{P}, \tag{C.9}$$

where $\mathcal{K}_i$ and $\mathcal{M}_{Ei}$ are the intrinsic and extrinsic parameters of camera $\mathbf{c}_i$ determined in Section 4.1. If the projected pixel $\mathcal{P}$ is located in the inner area of the particle profile in camera $\mathbf{c}_i$, then the corresponding point ${}^{W}\mathcal{P}$ is regarded as part of the 3-D particle and remained. In the contrary, the point ${}^{W}\mathcal{P}$, which projection is located outside the particle profile in camera $\mathbf{c}_i$, is discarded. The remaining point of volume V_i, is called the carved result under the camera $\mathbf{c}_i$. With new camera $\mathbf{c}_j$ incorporated, new carved result V_j can be obtained. The intersection of V_i and V_j is the carved result under camera $\mathbf{c}_i$ and camera $\mathbf{c}_j$.

As a result, for a carving process with n camera involved, the final intersection result can be obtained by

$$V_f = V_1 \cap V_2 \cap \cdots \cap V_n. \tag{C.10}$$

The final intersection result V_f is regarded as the 3-D approximation of the original object.

References

[1] B.J. Roylance, T.M. Hunt, The Wear Debris Analysis Handbook, Coxmoor publishing companys, Chipping Norton, 1999.
[2] S. Raadnui, Wear particle analysis utilization of quantitative computer image analysis: a review, Tribol. Int. 38 (10) (2005) 871–878.
[3] B. Roylance, D. Vaughan, Wear studies through particle size distribution ii: multiple field analysis in ferrography, Wear 90 (1) (1983) 137–147.
[4] B. Roylance, S. Raadnui, The morphological attributes of wear particles-their role in identifying wear mechanisms, Wear 175 (1) (1994) 115–121.
[5] M. Kumar, P. Shankar Mukherjee, N. Mohan Misra, Advancement and current status of wear debris analysis for machine condition monitoring: a review, Ind. Lubr. Tribol. 65 (1) (2013) 3–11.
[6] Z. Peng, T. Kirk, Z. Xu, The development of three-dimensional imaging techniques of wear particle analysis, Wear 203 (1997) 418–424.
[7] Y. Tian, J. Wang, Z. Peng, X. Jiang, A new approach to numerical characterisation of wear particle surfaces in three-dimensions for wear study, Wear 282 (2012) 59–68.
[8] G. Stachowiak, P. Podsiadlo, Towards the development of an automated wear particle classification system, Tribol. Int. 39 (12) (2006) 1615–1623.
[9] L.G. Gladkis, H. Timmers, J.M. Scarvell, P.N. Smith, Detailed three-dimensional size and shape characterisation of uhmwpe wear debris, Wear 270 (7) (2011) 455–463.
[10] A.K. Jardine, D. Lin, D. Banjevic, A review on machinery diagnostics and prognostics implementing condition-based maintenance, Mech. Syst. Signal Process. 20 (7) (2006) 1483–1510.
[11] Y. Peng, T. Wu, S. Wang, N. Kwok, Z. Peng, Motion-blurred particle image restoration for on-line wear monitoring, Sensors 15 (4) (2015) 8173–8191.
[12] R. Mat Dan, Multi-view and Three-dimensional (3D) Images in Wear Debris Analysis (WDA) (Ph.D. thesis), University of Manchester, Manchester, 2013.
[13] Y. Peng, T. Wu, S. Wang, Z. Peng, Oxidation wear monitoring based on the color extraction of on-line wear debris, Wear 332 (2015) 1151–1157.
[14] Y. Iwai, T. Honda, T. Miyajima, S. Yoshinaga, M. Higashi, Y. Fuwa, Quantitative estimation of wear amounts by real time measurement of wear debris in lubricating oil, Tribol. Int. 43 (1) (2010) 388–394.
[15] L. Du, J. Zhe, A high throughput inductive pulse sensor for online oil debris monitoring, Tribol. Int. 44 (2) (2011) 175–179.
[16] T. Wu, H. Wu, Y. Du, Z. Peng, Progress and trend of sensor technology for online oil monitoring, Sci. China Technol. Sci. 56 (12) (2013) 2914–2926.
[17] T. Wu, J. Mao, J. Wang, J. Wu, Y. Xie, A new on-line visual ferrograph, Tribol. Trans. 52 (5) (2009) 623–631.
[18] J. Tucker, A. Schultz, C. Lu, T. Sebok, C. Holloway, L. Tankersley, T. McClelland, P. Howard, J. Reintjes, Lasernet fines optical wear debris monitor, in: International Conference on Condition Monitoring, 1999, pp. 445–452.
[19] Z. Chen, T. Ellis, A self-adaptive gaussian mixture model, Comput. Vis. Image Underst. 122 (2014) 35–46.
[20] S.-K. Weng, C.-M. Kuo, S.-K. Tu, Video object tracking using adaptive kalman filter, J. Vis. Commun. Image Represent. 17 (6) (2006) 1190–1208.
[21] S. Chen, Kalman filter for robot vision: a survey, IEEE Trans. Ind. Electron. 59 (11) (2012) 4409–4420.
[22] K.-Y.K. Wong, R. Cipolla, Reconstruction of sculpture from its profiles with unknown camera positions, IEEE Trans. Image Process. 13 (3) (2004) 381–389.
[23] A.W. Fitzgibbon, G. Cross, A. Zisserman, Automatic 3d model construction for turn-table sequences, in: 3D Structure from Multiple Images of Large-Scale Environments, Springer, 1998, pp. 155–170.

[24] A. Sobral, A. Vacavant, A comprehensive review of background subtraction algorithms evaluated with synthetic and real videos, Comput. Vis. Image Underst. 122 (2014) 4–21.
[25] A. Vatavu, R. Danescu, S. Nedevschi, Stereovision-based multiple object tracking in traffic scenarios using free-form obstacle delimiters and particle filters, Intell. IEEE Trans. Transp. Syst. 16 (1) (2015) 498–511.
[26] E. Meijering, O. Dzyubachyk, I. Smal, et al., Methods for cell and particle tracking, Methods Enzymol. 504 (9) (2012) 183–200.
[27] X.R. Li, Y. Bar-Shalom, Tracking in clutter with nearest neighbor filters: analysis and performance, Aerosp. IEEE Trans. Electron. Syst. 32 (3) (1996) 995–1010.
[28] S.-Y. Park, M. Subbarao, Automatic 3d model reconstruction based on novel pose estimation and integration techniques, Image Vis. Comput. 22 (8) (2004) 623–635.
[29] Z. Zhang, Camera Calibration, Springer, Berlin, 2014.
[30] J.C. Russ, The Image Processing Handbook, CRC press, Boca Raton, 2015.
[31] G. Stachowiak, A.W. Batchelor, Engineering Tribology, Butterworth-Heinemann, Waltham, 2013.
[32] P. Campisi, K. Egiazarian, Blind Image Deconvolution: Theory and Applications, CRC Press, Boca Raton, 2016.